Journal of Experimental Botany, Vol. 73, No. 11 pp. 3807–3822, 2022
https://doi.org/10.1093/jxb/erac108 Advance Access Publication 17 March 2022

RESEARCH PAPER

Cold and exogenous calcium alter *Allium fistulosum* cell wall pectin to depress intracellular freezing temperatures

Jun Liu[1,†], Ian R. Willick[1,†], Hayato Hiraki[2], Ariana D. Forand[1], John R. Lawrence[3], George D.W. Swerhone[3], Yangdou Wei[4], Supratim Ghosh[5], Yeon Kyeong Lee[6], Jorunn E. Olsen[6], Björn Usadel[7,8], Alexandra Wormit[7], Markus Günl[8], Chithra Karunakaran[9], James J. Dynes[9], and Karen K. Tanino[1,*]

[1] Department of Plant Sciences, University of Saskatchewan, Saskatoon, SK, Canada
[2] The United Graduate School of Agricultural Sciences, Iwate University, Morioka, Japan
[3] Watershed Hydrology and Ecology Research Division, Environment and Climate Change Canada, Saskatoon, SK, Canada
[4] Biology Department, University of Saskatchewan, Saskatoon, SK, Canada
[5] Department of Food and Bioproducts Sciences, University of Saskatchewan, Saskatoon, SK, Canada
[6] Department of Plant Sciences, Faculty of BioSciences, Norwegian University of Life Sciences, Ås, Norway
[7] RWTH Aachen University, Institute for Biology I, Aachen, Germany
[8] IBG-2: Plant Sciences, Forschungszentrum Jülich, Germany
[9] Canadian Light Source, Saskatoon, SK, Canada

[†] These authors contributed equally to this work.
* Correspondence: karen.tanino@usask.ca

Received 26 October 2021; Editorial decision 7 March 2022; Accepted 14 March 2022

Editor: John Lunn, MPI of Molecular Plant Physiology, Germany

Abstract

De-methyl esterification of homogalacturonan and subsequent cross-linking with Ca^{2+} is hypothesized to enhance the freezing survival of cold acclimated plants by reducing the porosity of primary cell walls. To test this theory, we collected leaf epidermal peels from non- (23/18 °C) and cold acclimated (2 weeks at 12/4 °C) Japanese bunching onion (*Allium fistulosum* L.). Cold acclimation enhanced the temperature at which half the cells survived freezing injury by 8 °C (LT_{50} =–20 °C), and reduced tissue permeability by 70-fold compared with non-acclimated epidermal cells. These effects were associated with greater activity of pectin methylesterase (PME) and a reduction in the methyl esterification of homogalacturonan. Non-acclimated plants treated with 50 mM $CaCl_2$ accumulated higher concentrations of galacturonic acid, Ca^{2+} in the cell wall, and a lower number of visible cell wall pores compared with that observed in cold acclimated plants. Using cryo-microscopy, we observed that 50 mM $CaCl_2$ treatment did not lower the LT_{50} of non-acclimated cells, but reduced the lethal intracellular ice nucleation to temperatures observed in cold acclimated epidermal cells. We postulate that the PME-homogalacturonan-mediated reduction in cell wall porosity is integral to intracellular freezing avoidance strategies in cold acclimated herbaceous cells.

Keywords: Calcium, cell wall, cold acclimation, freezing, homogalacturonan, pectin methylesterase

Abbreviations: FTIR, Fourier-transform mid infrared spectroscopy;HG, homogalacturonan;LT_{50}, temperature at which half the cells survived freezing injury;PME, pectin methylesterase;RG-I, rhamnogalacturonan I;RG-II, rhamnogalacturonan II;XAS, X-ray absorption spectroscopy.

Introduction

Survival at temperatures below 0 °C is contingent on whether plants can tolerate extracellular ice nucleation or can depress the nucleation temperature to avoid freezing (Sakai and Larcher, 1987). Disruption of the plasma membrane after freeze-thaw injury in tolerant plants, or following intracellular ice nucleation in freezing avoidant plants, is generally accepted as the primary cause of lethal injury (Arora, 2018). A growing body of evidence, however, supports the theory that site-specific remodelling of the cell wall enhances survival at sub-zero temperatures (Panter *et al.*, 2019; Takahashi *et al.*, 2019, 2021*a*; Stegner *et al.*, 2020; Steiner *et al.*, 2020).

Early research incorporating plant protoplasts surmised that the attachment of the plasma membrane to the cell wall can exacerbate cellular injury (Siminovitch *et al.*, 1978; Murai and Yoshida, 1998). Observations from artificial cell wall matrices (Olien, 1974; Ashworth and Abeles, 1984) and intact plant tissues (George and Burke, 1977; Wisniewski and Davis, 1995; Rajashekar and Lafta, 1996; Yamada *et al.*, 2002) indicate that the cell wall can impede the propagation of ice. Ashworth and Abeles (1984) hypothesized that ice nucleation through a cell wall microcapillary will only occur when temperatures decline below the melting point of water, as determined by the diameter of the pore. The evaporative loss or freezing of intracellular water is therefore proportional to cell wall pore size (George and Burke, 1977; Ashworth and Abeles, 1984). Recent evidence supports the theory that site-specific variability in cell wall composition is an adaptive mechanism that promotes the expansion or collapse of cells to tolerate the formation of ice aggregates, or reduce cell wall porosity to promote supercooling and impede ice propagation (Schott *et al.*, 2017; Stegner *et al.*, 2020; Steiner *et al.*, 2020; Takahashi *et al.*, 2021*b*).

Plant cell walls are comprised of a middle lamella, a primary and secondary cell wall. The middle lamella is predominately homogalacturonan (HG) pectin (Zamil and Geitmann, 2017). In contrast, the primary cell wall is composed of cellulose microfibrils interspersed with hemicelluloses such as xyloglucan, embedded proteins and pectin polysaccharides such as HG, xylogalacturonan, rhamnogalacturonan I (RG-I), and rhamnogalacturonan II (RG-II). Secretion of a lignified secondary cell wall can occur after the cessation of growth and is present in tissues that require structural reinforcement (Meents *et al.*, 2018). Cell wall mutant studies led to the hypothesis that localized biomechanical hotspots containing xyloglucans manipulate the mechanical properties of plant cell walls (Park and Cosgrove, 2015; Xiao *et al.*, 2016). These junctions promote slippage and stress relaxation by the action of expansins and cell wall loosening proteins (Cosgrove, 2018). Nuclear magnetic resonance spectroscopy of Arabidopsis leaves further identified pectin-forming gels and tight associations with cellulose that may contribute to the biomechanical hotspots (Wang *et al.*, 2015), or form a separate set of linkages between cellulose microfibrils (White *et al.*, 2014).

Although our current understanding of the pectin-cell wall structural complex may change (Mohnen *et al.*, 2021), the prevailing view is that the majority of cell wall pectins are linear chains of HG containing a backbone of partially methyl esterified (1-4)-α-D-galacturonic acid (Zamil and Geitmann, 2017). Regions of HG are covalently linked with arabinogalactan proteins and branching pectic polymers of RG-I and RG-II. De-methyl esterification of HG *in muro* by pectin methylesterase (PME, EC. 3.1.1.11), through the hydrolysis of the methyl ester bond at the C-6 position on galacturonic acid in a linear block-wise fashion, results in a continuous region of de-methyl esterified HG that can be cross linked by Ca^{2+} to form a semi-rigid pectate gel (Willats *et al.*, 2001). A low degree of HG methyl esterification can also facilitate the acetylation or substitution of galacturonic acid with other subunits (Atmodjo *et al.*, 2013) and enhance interactions with cellulose microfibrils to rigidify plant tissues (Phyo *et al.*, 2017). De-methyl esterification of HG does not necessarily reduce cell wall permeability and porosity. Random de-methyl esterification by PME can occur and is less effective at forming rigid pectate gels (Willats *et al.*, 2001). Exposure of common onion (*Allium cepa* L.) epidermal cells to PME in the absence of exogenous Ca^{2+} treatment promoted swelling (hydration) of the cell wall. A combination of exogenous Ca^{2+} and PME reduced cell wall plasticity (Wang *et al.*, 2020).

Plants can enhance their capacity to tolerate or avoid freezing injury through exposure to declining photoperiods and low threshold temperatures (Weiser, 1970). During cold acclimation, plants shift protein and metabolite profiles, redistribute tissue water, and re-model the cell wall and plasma membrane (see Gusta and Wisniewski, 2013; Shi *et al.*, 2018; Takahashi *et al.*, 2018, 2021*b*) for recent reviews). The cold acclimation-induced accumulation of cell wall dry matter (Griffith *et al.*, 1985; Tanino *et al.*, 1990; Solecka *et al.*, 2008) corresponded with the deposition of lipid bodies (Griffith *et al.*, 1985), the accumulation of sucrose (Tanino *et al.*, 1990), pectins and hemicelluloses (Kubacka-Zębalska and Kacperska, 1999; Baldwin *et al.*, 2014; Willick *et al.*, 2018; Takahashi *et al.*, 2021*a*) and a shift in apoplastic protein composition (Willick *et al.*, 2018; Takahashi *et al.*, 2019). Exposure of winter rape (*Brassica napus* subsp. *oleifera*) to cold acclimation conditions specifically determined de-methyl esterification of HG, enhanced tissue rigidity, and corresponded with a greater capacity to tolerate freezing injury (Kubacka-Zębalska and Kacperska, 1999; Solecka *et al.*, 2008).

This study assessed whether cold acclimation or the exogenous soil application of $CaCl_2$ enhanced freezing survival through the Ca^{2+} cross-linking of HG. We employed a single cell layer epidermal peel from a perennial Japanese bunching onion (*Allium fistulosum* L.) as a model system due to the relative ease to isolate a single cell layer and large cell size (250–400 μm × 50 μm × 90 μm). Epidermal cell layers from common

onion were utilized to assess freezing injury (Palta *et al.*, 1977; Arora and Palta, 1986, 1988), cell wall loosening, and softening (Wang *et al.*, 2015; Cosgrove, 2018; Wang *et al.*, 2020). However, the Japanese bunching onion has advantages over the common onion system, including a constitutive freezing tolerance of −13 °C (Tanino *et al.*, 2013) that is comparable to the freezing tolerance of cold acclimated common onion (Palta *et al.*, 1977; Arora and Palta, 1986, 1988), and a capacity to survive up to −27 °C after only 14 d at 4 °C (Tanino *et al.*, 2013). The objective of this work was to explore whether Ca^{2+} cross-linking of HG through $CaCl_2$ application or cold acclimation inhibits intracellular freezing and enhances the overall freezing tolerance of Japanese bunching onion epidermal cells.

Materials and methods

Plant material and acclimation treatments

Japanese bunching onion (*Allium fistulosum* L.) seeds harvested in Saskatoon, SK Canada (52°7 N, 106°4 W) were grown for 3 months in 15 cm diameter pots with soilless mix (Sunshine No. 4, Sungro Hort Inc, Bellvue, WA, USA) at (20 ± 5 °C) under natural light supplemented with 400 W high-pressure sodium lights (18 h photoperiod, average of 600 μmol m^{-2} s^{-1}). Non-acclimated plants were supplemented with 100 ml of water and calcium-fortified plants were supplemented with 100 ml of 0.05 M $CaCl_2$ solution every 2 d over a 28 d period. To induce cold acclimation, plants were transferred for 14 d to a growth chamber (Conviron, Winnipeg, MB, Canada) set to 12 °C/4 °C (day/night) with an 8 h photoperiod and a light intensity of 370 μmol m^{-2} s^{-1}.

Assessment of protoplasmic streaming and cell survival

Stems with attached leaves were transferred to 50 ml test tubes containing 2 ml of distilled water. In total, per treatment, five stems with attached leaves in tubes were transferred to an ethylene glycol low temperature bath (Neslab Endocal RTE-Series, Portsmouth, NH, USA) held isothermal at −2.5 °C for 30 min, before inducing nucleation with ice shavings. The bath was cooled to and held at −5 °C for 2 h before cooling samples at a rate of −5 °C h^{-1}. Samples were transferred after 1 h at −10 °C, −15 °C, −20 °C, −25 °C, and −30 °C to a 4 °C dark room overnight. Thawed stems with leaves were warmed to room temperature (24 °C) for 1 h. Three peels per stem and ten cells per peel were assessed for the presence (alive) or absence (dead) of protoplasmic streaming, as described by Tanino *et al.* (2013).

Apoplast permeability

Epidermal layers from five plants per treatment were submerged for 16 h at 20 °C in 5 mg ml^{-1} solutions of a mixture of 3000–70 000 MW dextran molecules which were conjugated with fluorescein (Sigma-Aldrich Chemical Co. St. Louis MO, USA) in 0.1 M Phosphate buffered saline (pH 7.2), and observed with a confocal laser scanning microscope (CLSM; Zeiss LSM 510 Confor2, Germany; modified from Jones *et al.*, 2000).

In a separate experiment using unconjugated, fluorescein molecules alone (5.02 Å radius, Mustafa *et al.*, 1993; 6.5 Å radius, Lawrence *et al.*, 1994) we quantified the diffusion rate of fluorescein from the extracellular to the intracellular space using a Nikon Eclipse 80I CLSM (Nikon Instruments Inc., Melville, NY, USA) as described by Liu (2015). A cover well was placed upside down, the abaxial side of the epidermis was placed on the glass surface, glass wool was placed on top of the epidermis to hold it in place, a microscope slide was placed on top, and then pressed into place. The slide was transferred to the CLSM, cover well side up, and the focus was set to 30 μm from the cell wall (the approximate mid-point). A 100 μl aliquot of 1 mg ml^{-1} fluorescein solution was injected through the injection port in the cover glass. The diffusion rate was assessed at 10 s intervals using NIS Elements software (Nikon Instruments Inc., Melville, NY, USA) by counting the saturated pixels in the image and quantifying the slope of the saturated pixels over time.

Pectin methylesterase (PME) activity

Cell walls, soluble and insoluble cell wall proteins from five plants per treatment were extracted as described by Solecka *et al.* (2008) and assessed for protein concentration using the Bio-Rad assay kit, according to the manufacturer's instructions (Berkeley, CA, USA). The activity of PME was assessed as described by Richard *et al.* (1994) with reaction mixtures containing 0.5% (w/w) highly methyl esterified citrus pectins (Sigma Chemical Co. St. Louis, MO, USA), 0.2 M NaCl and 0.015 (w/v) methyl red as a pH indicator. A 5 μl protein extract was added to 950 μl of the reaction mixture and measured spectrophotometrically (GENESYS 10 Bio, Thermo Fisher Scientific, Madison, WI, USA) at 525 nm for 2 min at 25 °C. A calibration curve was generated by adding HCl to obtain 1–200 nEq H^+ to 1 ml of the reaction mixture, and the enzyme activity was standardized per mg of protein as described by Solecka *et al.* (2008). Tissue PME activity was expressed where one unit of PME activity was defined as one nano-equivalent of protons (nEq H^+) released per mg of protein per min.

Fourier transform mid-infrared (FTIR) spectroscopy

Onion epidermal peels were deposited and air-dried flat on 3 mm thick BaF_2 circular slides. FTIR spectroscopy was performed at the Canadian Light Source Inc. (Saskatoon, SK, Canada). The absorbance spectra from polygalacturonic acid, 55% methylesterified and 85% methylesterified pectin (Sigma-Aldrich, Toronto, ON, Canada) were measured in the transmission mode using the spectrometer with globar (silicon carbide) source. A Bruker—IFS 66V/S spectrometer (Bruker Optics, Ettlingen, Germany) with a liquid nitrogen cooled Deuterated triglycine sulphate detector was used for the transmission measurements. To record the spectra, pectin standards or KBr (control) were ground to a powder with 99 mg of KBr, and compressed into a 13 mm diameter pellet, as described by Willick *et al.*, 2020. Three pellets made from random sampling for each sample were used to collect the infrared spectra. All infrared data were collected in the mid infrared region (4000–800 cm^{-1}) with a spectral resolution of 2 cm^{-1}. The sample chamber was evacuated to minimize the intense spectral peaks due to absorption by CO_2 and H_2O. Each sample spectrum was an average of 64 scans, and pure KBr pellet spectrum (average of 512 scans) was recorded for normalizing all sample spectra.

All data analysis of the reference samples was performed using the OPUS (version 7.2, Bruker Optics Inc., Billerica, MA, USA) software. Spectra were averaged and a 64 point rubber-band baseline correction was applied so the minima in each spectral region of interest fit a convex polygonal line that are then subtracted from the original spectra baseline (Willick *et al.*, 2020). The second derivatives of each spectra were smoothed using nine points and Origin (version 9.1, OriginLab Corporation, MA, USA) was used to plot all the spectral data. The area under absorption bands were determined using the method B in OPUS.

The infrared spectromicroscopy data of dried onion cells were collected using the Bruker Hyperion imaging microscope equipped with a 64 × 64 MCT (Mercury-Cadmium-Telluride) Focal Plane Array (FPA) detector. A 15× objective lens was used and the spatial resolution per pixel when using this objective lens was 2.7 × 2.7 $μm^2$. The spectra were collected at a resolution of 4 cm^{-1} and were an average of 256 scans $pixel^{-1}$. Background spectra were collected from a clean region

in the BaF_2 windows, averaged over 512 scans. All sample data were normalized using the background spectrum. Nine spectra from selected regions around the cell walls were extracted from two biological replicates of non-acclimated and cold acclimated samples. The principal component analysis was performed on multiple spectra from the replicate samples of non-acclimated and cold acclimated treatments using Unscrambler (version 10.1, Camo Software AS., Norway). The average of non-acclimated and cold acclimated samples were used to determine the degree of de-methylation.

X-ray absorption spectroscopy (XAS) analysis of Ca^{2+}

The XAS measurements were carried out on the Spherical Grating Monochromator beamline 11ID-1 at the Canadian Light Source in Saskatoon (Regier *et al.*, 2007). Epidermal peels from three plants per treatment were mounted on the sample holder and dried in a desiccator at 21 °C. Calcium L-edge partial fluorescence yield XAS spectra were recorded using a single energy-resolved Amptek Silicon Drift Detector and step scanning at 48 s $point^{-1}$. The spectra were normalized using the drain current from a gold mesh and are the average of two scans. Calibration of the spectra utilizes the characteristic strong L_2-edge absorption peak at 352.5 eV, as described by Cosmidis *et al.* (2015).

Antibody labelling

Samples from four plants per treatment were prepared for immunofluorescence labelling, as described by (Lee *et al.*, 2008). Samples were blocked with a phosphate-buffered saline solution containing 3% (w/v) milk protein and incubated at 21 °C for 30 min. The antibodies JIM5, which recognizes partially methyl esterified, and JIM7, which recognizes heavily methyl esterified epitopes of HG (PlantProbes, Leeds, UK) diluted 10× in 0.1 M phosphate-buffered saline (pH 7.2), were bound to the wall surface for 1 h followed by the addition of fluorescein isothiocyanate-linked anti-rat IgG (Abcam, Cambridge, MA, USA) for an additional 1 h. Sections were washed three times in 0.1 M phosphate-buffered saline (pH 7.2) for 5 min at the end of each antibody labelling step. Labelled samples were mounted with a prolonged gold antifade reagent (Life Technologies, Carlsbrad, CA, USA) and imaged using an Evos digital inverted fluorescent microscope (Thermo Fisher Scientific, Madison, WI, USA). All incubation steps were performed in the dark and at 21 °C.

Cell wall compositional analysis

Material from three plants per treatment was frozen with liquid nitrogen and lyophilized. Alcohol insoluble residues (AIR) were extracted and prepared for monosaccharide analysis by gas chromatography mass spectrometry, as described by (Foster *et al.*, 2010) with minor modifications. Approximately 2 mg of AIR was extracted twice with 800 µl water by shaking for 15 min at 60 °C (yielding the water-soluble cell wall fraction). The supernatants were pooled and hydrolysed with the equivalent of one volume of 4 M trifluoroacetic acid (TFA) for 90 min at 121 °C in a heating block. The TFA was evaporated under a gentle stream of air and the samples were further processed for GC-MS analysis, as described by (Foster *et al.*, 2010). The remaining cell wall material (after extraction with water) yielded the insoluble cell wall fraction, and the samples were prepared according to (Foster *et al.*, 2010). Samples were injected into a gas chromatogram equipped with a quadrupole mass spectrometer (Agilent Technologies, Santa Clara, CA, USA), with a 30 × 0.25 mm × 0.25 µm Supelco SP-2380 column (Sigma Aldrich, St. Louis, MO, USA), 4 min solvent delay and a flow rate of 1.5 ml min^{-1}. Injected samples were subjected to the following temperature program: initial hold at 160 °C for 2 min; a 20 °C min^{-1} ramp to 200 °C and hold for 5 min; a 20 °C min^{-1} ramp to 245 °C and hold for 12 min; spike to 270 °C and hold for 5 min, before cooling to the initial temperature of 160 °C. Monosaccharide peaks were identified by mass profiles and the retention times derived from standard solutions, and quantified based on standard curves.

Cryo-microscopy

Using a cryo-stage (Linkam freezing stage, LTS 120, Scientific Instruments, Waterfield, UK) we characterized ice nucleation in five onion epidermal peels per treatment. Protoplasmic streaming was confirmed before analysis in each epidermal peel. The cryo-stage apparatus (Linkam PE94; Scientific Instruments, Waterfield, UK) was connected to a Nikon E400 light microscope with a Nikon DS-Fi1 camera (Nikon Canada Inc., Mississauga, ON, Canada). Extrinsic ice nucleation in the extracellular space was induced by adding a drop of 10 mg silver iodide powder resuspended in 10 ml water to the glass slide and the onion epidermal layer was placed over the suspension. The temperature of the cryostage was then lowered from 0 to −2.5 °C and held for 2 h to initiate ice nucleation. The cryo-stage was cooled at a rate of 5 °C h^{-1} to −23 °C. The temperature at which intracellular ice nucleation subsequently occurred was recorded, and was based on shifts in light refraction of the symplasm upon freezing. The cryostage was subsequently warmed to 20 °C and held at that temperature for at least 0.5 h before observations were recorded on protoplasmic streaming.

Light microscopy

Epidermal peels collected from four plants per treatment were cut into 4 cm^2 sections and immersed on slides containing a solution of 2% Alizarin red S (Sigma-Aldrich Canada Co., Oakville, ON, Canada) in distilled water, pH 4.2, for 5 min, and then samples were washed with 0.1 M phosphate buffered saline solution. The presence of crimson precipitates indicated concentrations of Ca^{2+} above a surface density of 0.002 µg mm^{-2} (Paul *et al.*, 1983). Stained sections were mounted in phosphate buffered saline and imaged using a LEICA DM4B microscope with a LEICA DFC7000T camera (Wetslar, Germany). The diameter of the crimson precipitates was assessed with ImageJ (version 1.3.1093, National Institute of Health, USA) to assess the relative thickness of the Ca^{2+}-associated region within the cell wall.

Electron microscopy

Epidermal peels from four plants per treatment were fixed in 2% glutaraldehyde in 0.1 M sodium cacodylate (pH 7.4) overnight, washed with 0.1 M sodium cacodylate and stored at 4 °C. Prior to scanning electron microscopy, samples were dehydrated with a graded ethanol series, critical point dried (Polaron E3000, East Sussex, UK), sputter-coated with 5 nm Chromium (Quorum Q150T ES, East Sussex, UK) and imaged with a scanning electron microscope (Hitachi SU8010 FE-SEM; Hitachi, Tokyo, Japan). For transmission electron microscopy, four fixed samples per treatment were exposed to 1% osmium tetroxide for 1 h at 21 °C, rinsed with water, dehydrated through a graded ethanol series, and infiltrated through graded London Resin White (Agar Scientific Ltd., Stansted, Essex, UK) in ethanol series, as described by Lee *et al.* (2008). Samples transferred to Pure London Resin White were polymerized at 50 °C for 24 h. A 90 nm section was mounted on 200 mesh copper grids, critical point dried and then stained with a 2% uranium acetate and Reynolds lead citrate solution. Sections were examined using Hitachi HT7700 Transmission Electron Microscope (Tokyo, Japan). Images captured from SEM were processed by the threshold function of ImageJ to convert the pores to black pixels, and other portions became white. The number of pores were counted using the 'analyse particle' function. Particle size was set to detect regions of interest greater than 15 pixels to exclude very small pores or particles. For the TEM images, the un-modified grey images were processed using the threshold function to emphasize the cell layer morphology.

Data analysis

The degree of methyl esterification was determined using the OPUS integration method C (version 7.0, Bruker Optics Inc., Billerica, MA, USA) wherein the area under the 1740 cm^{-1} methylation peak was determined after considering two baseline points at 1770 and 1710 cm^{-1}. The LT_{50} for each independent experiment was calculated by fitting survival data to Gompertz sigmoidal curves, as described by (Kovaleski and Grossman, 2021). Analyses of mean LT_{50s} and monosaccharide concentrations were performed using Sigmaplot (version 12.5, Systat Software Inc., Chicago, IL, USA) one-way analysis of variance procedure with Tukey's test. Two-tailed *t*-tests determined differences between the means of ice nucleation temperatures, tissue permeability, methyl peak integrated areas, thickness of the cell wall region containing Ca^{2+} deposits, and the number of visible cell wall pores in electron micrographs.

Results

Cold acclimation enhances cell freezing tolerance and reduces tissue permeability

The LT_{50} electrolyte leakage test revealed significant differences ($P<0.05$) in the cold acclimation capacity of Japanese bunching onions (Fig. 1). Epidermal peels collected from Japanese bunching onions grown at 12 °C/4 °C (day/night) for 14 d developed an LT_{50} of −20°C, while plants cold acclimated for 7 d had an LT_{50} of −16.5°C with non-acclimated plants at an LT_{50} of −12°C. Subsequent experiments denoting cold acclimation refer to a 12 °C/4 °C (day/night) exposure time of 14 d.

Administration of a fluorescein-linked dextran tracer solution (13 Å radius) assessed the influence of cold acclimation on epidermal peel tissue permeability. Fluorescence was observed in the apoplast and cytoplasm of non-acclimated epidermal cells, indicating that the fluorescein-conjugated dextrans penetrated the cell wall of epidermal peels from non-acclimated plants (Fig. 2A). In contrast, fluorescence in the epidermal peels from cold acclimated plants was visibly less pronounced and did not appear to cross the apoplast (Fig. 2B). The smaller non-conjugated fluorescein (5.02 Å radius) was able to diffuse across the cell wall to the midpoint of the intracellular space (30 µm depth) in epidermal peels collected from non-acclimated plants at a rate of 29 pixels s^{-1}, 70-fold faster compared with epidermal peels collected from cold acclimated Japanese bunching onions (Fig. 2C). The smaller fluorescein molecule could easily penetrate all regions of the extracellular and intracellular space of non-acclimated cells, but the rate of penetration was significantly reduced ($P<0.01$) in cold acclimated cells.

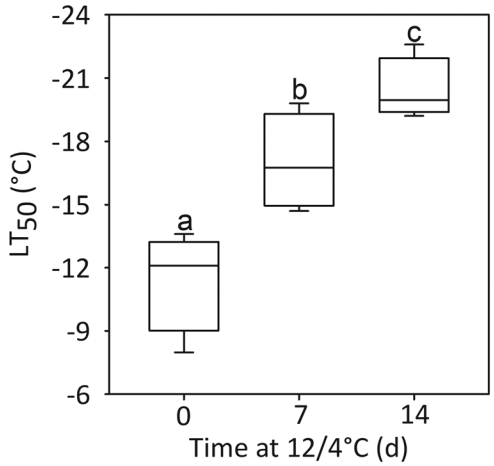

Fig. 1. The lethal temperature at which half of cold acclimated epidermal cells recovered from freezing injury (LT_{50}). Japanese bunching onion were cold acclimated at 12/4 °C for 0, 7 or 14 d. Data are presented as a medians of four independent experiments (n= 4; three plants per temperature per treatment in each LT_{50} experiment). Medians followed by the same letter were not significantly different based on Tukey's test (One-way ANOVA, $P<0.05$).

Cold acclimation alters cell wall composition

The cold acclimation of Japanese bunching onion resulted in a 1.8-fold higher accumulation of epidermal cell wall dry matter (Fig. 3A), 1.4-fold higher total protein abundance (Supplementary Fig. S1), a decline in soluble PME activity (Fig. 3B), and a 2.3-fold higher cell wall (insoluble) PME activity (Fig. 3C). Higher total PME enzyme activity in response to cold acclimation was driven by the PME activity of the cell wall bound fraction of the epidermal layer (Fig. 3B-D).

Cold acclimation-induced shifts in pectin methylation status were visually assessed using monoclonal antibodies for partially (JIM5) and heavily (JIM7) methyl esterified epitopes of HG (Fig. 4A; Clausen *et al.*, 2003). Fluorescence was visibly low in the epidermal cell walls of non-acclimated Japanese bunching onion incubated with JIM5 (Fig. 4A), compared with cells collected from cold acclimated plants. Peels from non-acclimated and cold acclimated onions treated with JIM7 produced visibly comparable intensities of fluorescence in the cell wall.

Bands associated with the different chemical groups in the FTIR fingerprint region (1800–800 cm^{-1}; Fig. 4B), include the C=O and N-H vibrations corresponding with amide I (1655 cm^{-1}), N-H and C-N vibrations corresponding with amide II (1546 cm^{-1}), C-C and C-H stretching corresponding with cellulose (1350–1315 cm^{-1}), C-O-C stretching vibrations associated with glycosidic bonds between uronic acids (1150 cm^{-1}), C-O and C-C bonds of glucans (1070 cm^{-1}), and C-H deformations associated with glucans and cellulose (1030 and 970 cm^{-1}; Alonso-Simón *et al.*, 2011; Willick *et al.*, 2020). While spectral frequencies in the cell walls of cold acclimated Japanese bunching onion epidermal peels associated with cellulose (1350–1315 cm^{-1} and 970 cm^{-1}) visibly declined, frequencies associated with uronic acid (1740 cm^{-1} and 1150 cm^{-1}) were visibly greater in comparison with the same ranges in the cell walls of non-acclimated plants (Fig. 4B).

Within the FTIR fingerprint region (1800–800 cm^{-1}; Fig. 4B), two characteristic bands near 1749 and 1630 cm^{-1} can determine the number of esterified carboxylic groups relative to the total number of carboxylic groups (Willick *et al.*,

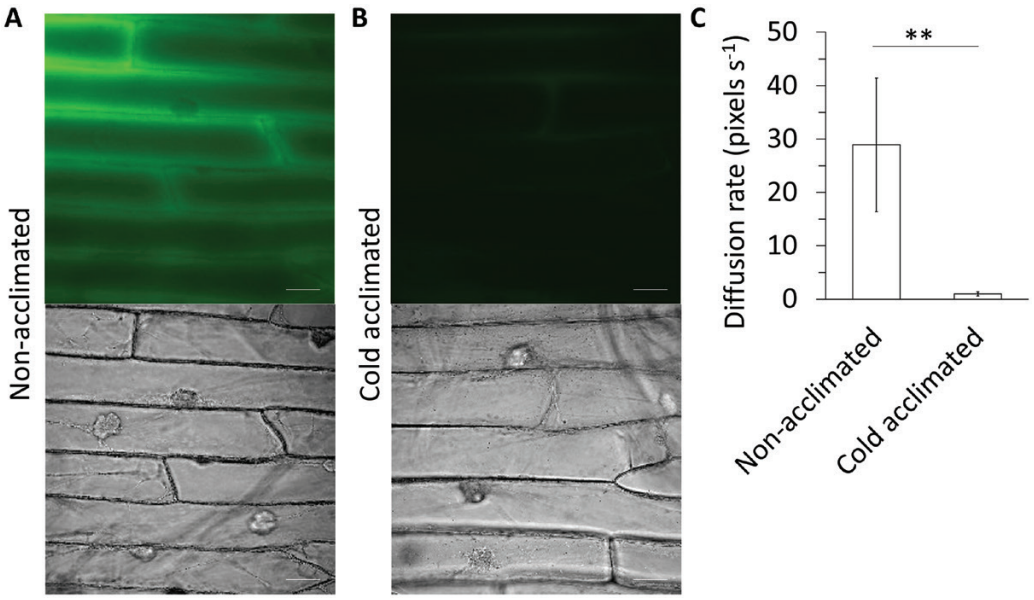

Fig. 2. The impact of cold acclimation on the permeability of Japanese bunching onion epidermal tissues when exposed to fluorescein dye molecules which were conjugated with a mixture of dextran sizes (3000 to 70 000 MW). Representative confocal (top panels) and brightfield (lower panels) microscopy images from five independent replicates of (A) non-acclimated and (B) cold acclimated epidermal peels. Paired images were captured with identical light intensities and camera exposure settings. Scale bar =50 μm. (C) The mean diffusion rate of non-conjugated fluorescein (5.02 Å radius) from the extracellular space to the midpoint of the intracellular space from three independent experiments (n= 3; five plants per acclimation treatment in each experiment). Means ±SD were determined to be statistically different using the Student's t-test (asterisks represent significant values, **, P<0.01).

2020). Using the ratio of area of the band at 1749 cm^{-1} (1830–1695 cm^{-1}) to the total area between bands of 1749 cm^{-1} and 1630 cm^{-1} (1695–1570 cm^{-1}), we determined the degree of esterification of polygalacturonic acid, high and low methylated pectin standards to be 100, 77, and 41%, respectively (Fig. 4C). The peaks identified in the pectin standards in this study align with previously published results (Chatjigakis *et al.*, 1998). The highly methylated pectin standard has the strongest absorption of $\nu_s(CH_3)$ bands at 2958 and 2856 cm^{-1} followed by low methylated pectin. Neither of these bands were present in the polygalacturonic acid standard. The ester band of the carboxyl group (1740 cm^{-1}) in the highly methylated pectin standard (1771–1712 cm^{-1}) is broad and shifted towards a higher wavenumber as compared with the band in low methylated pectin (1767–1725 cm^{-1}; Fig. 4C). As the methylation of pectin decreases, the ester peak shifts towards lower wavenumber (Szymanska-Chargot and Zdunek, 2013).

Principal component analysis of the spectral data indicated that the most important variations between spectra collected from non-acclimated and cold acclimated epidermal peels were explained in PC1 (60.4 %) and PC2 (31.2 %; Supplementary Fig. S2). Peaks within the FTIR fingerprint region contributing most to this variation were those between 1740–1721 cm^{-1}, and 1162–980 cm^{-1}. The 1740 cm^{-1} methyl esterification peak in the cell walls of cold acclimated Japanese bunching onion maintained a 2.3-fold lower intensity (P<0.001) compared with the cell walls of non-acclimated plants (Fig. 4D). A doublet peak at 1751 and 1735 cm^{-1} in cold acclimated Japanese bunching onion epidermal cell walls indicates that either two different types of esters may be present in the sample (Chatjigakis *et al.*, 1998), or the confirmation of change from high to low methylated pectins in cold acclimated samples; this is in agreement with the pectin reference spectra and other published work (Szymanska-Chargot and Zdunek, 2013). A lower methylation status in cold-acclimated epidermal onion cell walls corresponded with a visibly higher Ca^{2+} L-edge peak intensity (Supplementary Fig. S3).

Cold acclimation or $CaCl_2$ treatment modifies cell wall monosaccharide composition

Not surprisingly, the insoluble cell wall fraction contained a higher concentration of cell wall monosaccharides, compared with the water-soluble fraction (Table 1). Japanese bunching onions exposed to cold acclimation accumulated significantly higher concentrations of galacturonic acid in the soluble or insoluble fraction (P<0.05), compared with the same plants grown under non-acclimated conditions. Conversely, the application of 50 mM $CaCl_2$ did not enhance insoluble galacturonic acid accumulation in non-acclimated or cold acclimated Japanese bunching onions. Furthermore, epidermal peels from non-acclimated plants treated with an additional 50 mM $CaCl_2$ accumulated comparable concentrations of soluble galacturonic acid as the cold acclimated plants treated with or without $CaCl_2$. Onions grown under non-acclimated conditions and lacking the 50 mM $CaCl_2$ soil treatment accumulated higher

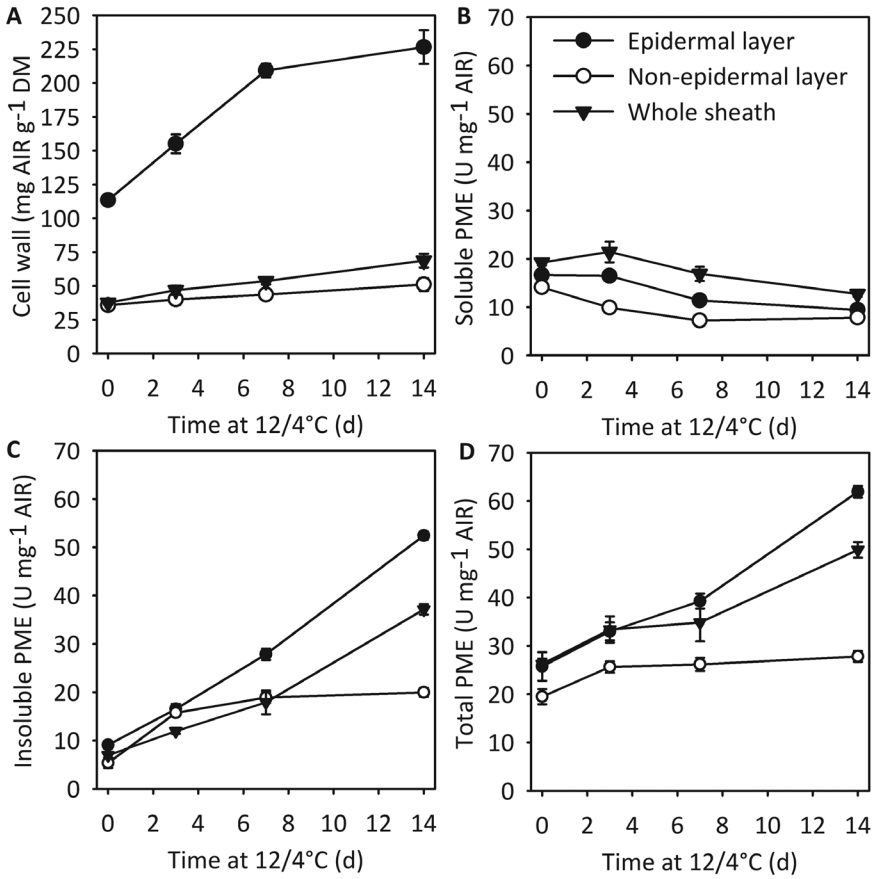

Fig. 3. Accumulation of cell wall dry matter and enhanced pectin methylesterase (PME) activity during the cold acclimation of Japanese bunching onion. (A) Cell wall alcohol insoluble residues (AIR) and PME activity in the (B) soluble, (C) wall-bound and (D) total fractions. Data are presented as means ±SD of four independent experiments (n=4; three plants per treatment in each experiment).

concentrations of insoluble glucose and xylose. All other tested monosaccharides did not shift in composition in response to cold acclimation or $CaCl_2$ treatment (Table 1).

Fortification with $CaCl_2$ modifies the propagation of ice across the cell wall and the capacity to survive freezing

Ice nucleation in all instances commenced from the extracellular space (Table 2). Ice aggregation in the extracellular space was denoted by a darkening of tissue radiating from the extracellular space (Supplementary Video S1, S2). Within 4 s of extracellular ice formation in non-acclimated cells, the plasma membrane contracted from the cell wall and the intracellular contents of cells froze independently of one another (Supplementary Video S1). In non-acclimated cells treated with 50 mM $CaCl_2$, extracellular ice initiated the propagation of ice along the surface of the epidermal layer and not into the intracellular space (Supplementary Video S2). The application of silver iodide triggered ice nucleation between –2.5 °C and –4 °C and delayed intracellular ice nucleation in cells from cold acclimated and non-acclimated 50 mM $CaCl_2$ treated plants (Table 2). In the absence of silver iodide, extracellular ice nucleated at lower sub-zero temperatures and intracellular water nucleated at comparatively warmer sub-zero temperatures (Table 2).

Interestingly, non-acclimated Japanese bunching onion supplemented with 50 mM $CaCl_2$ developed cells that supercooled to temperatures below –20 °C (Table 2). This is a 12 °C shift in the intracellular supercooling temperature from non-acclimated plants lacking the $CaCl_2$ treatment. Epidermal cells of non-acclimated plants supplemented with 50 mM $CaCl_2$ attained an LT_{50} of –12.9 °C which was only 2.4 °C lower compared with the LT_{50} attained by non-acclimated plants. Similarly, the cells of cold acclimated plants treated with 50 mM $CaCl_2$ attained an LT_{50} of –26.0 °C, which was 2.3 °C lower than the LT_{50} of cold acclimated plants lacking the $CaCl_2$ treatment (Fig. 5). Low intracellular ice nucleation temperatures in the epidermal cells of non-acclimated plants treated with 50 mM $CaCl_2$ was comparable to those in cold acclimated cells, despite a 10.4 °C higher LT_{50}. In contrast, the epidermal cells of cold acclimated plants without, and treated with, 50 mM $CaCl_2$ attained an LT_{50} (Fig. 5) that was comparable to the intracellular ice nucleation temperature of cold acclimated Japanese

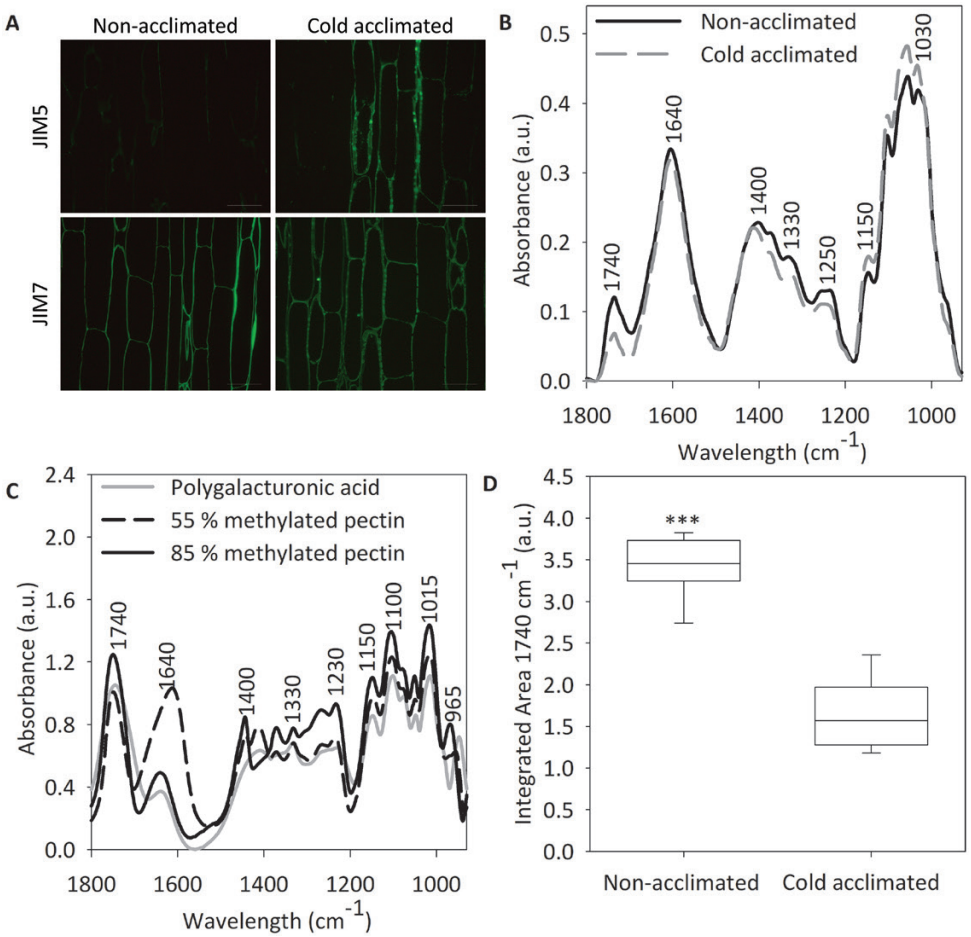

Fig. 4. Cold acclimation induced de-esterification of HG in Japanese bunching onion epidermal cell walls. (A) Immunolabelling of non-acclimated and cold acclimated epidermal cells with JIM5 and JIM7 antibodies detect partially and heavily methyl esterified epitopes of HG, respectively. Images were captured with identical exposure settings and light intensities. Scale bar =100 μm. Representative images from two independent experiments (three plants per acclimation treatment in each experiment). FTIR spectra were extracted from (B) non- and cold acclimated onion epidermal cell walls, (C) pectin standards. (D) The degree of methyl esterification (1740 cm^{-1}) as determined from FTIR absorbance spectra assessed from nine spectra collected from two plants per treatment (n=9, two-tailed t-test. Asterisks represent significant values, ***, P<0.001).

bunching onion epidermal cells extrinsically nucleated with AgI (Table 2).

Application of $CaCl_2$ modifies cell wall ultrastructure and the deposition of Ca^{2+} in the cell wall

We assessed microscopically whether the addition of 50 mM $CaCl_2$ in the nutrient solution enhanced the deposition of Ca^{2+} in the cell wall (Fig. 6A, B). The average thickness of the Ca^{2+} region was 2.5-fold higher (P<0.01) in $CaCl_2$-treated plants (Fig. 6C). Using scanning electron microscopy and image analysis, we characterized the number of pores (>15 pixels) on the cell wall surface (Fig. 7). There were approximately 100 pores associated with the epidermal cell wall of non-acclimated plants (Fig. 7A, D) and in comparison, 10-fold fewer pores (P<0.01) were observed in the epidermal cells of cold acclimated (Fig. 7B, D) and non-acclimated plants treated with 50 mM $CaCl_2$ (Fig. 7C, D). The side wall of epidermal cells in non-acclimated plants exhibited a flat surface on the interior cytoplasmic side (Fig. 8A, D). In contrast, the epidermal cells from cold acclimated plants developed an undulating surface with multiple cell wall layers (Fig. 8B, E). While the cells from non-acclimated plants treated with $CaCl_2$ displayed multiple cell wall layers, they did not develop an undulating interior surface (Fig. 8C, F).

Discussion

Effect of cold acclimation on the freezing tolerance and permeability of epidermal cells

The perennial Japanese bunching onion, *Allium fistulosum,* survives at sub-optimal overwintering conditions as evident by its capacity to tolerate prolonged exposure to sub-zero soil

Table 1. Analysis of water-soluble and insoluble epidermal cell wall monosaccharides from Japanese bunching onions exposed to non-acclimated (NA) or cold acclimated conditions, and plants treated with 50 mM $CaCl_2$ (+ Ca).

Monosaccharide (μg mg^{-1} AIR)	Non-acclimated	Non-acclimated + Ca	Cold acclimated	Cold acclimated + Ca
Insoluble				
Fucose	1.6 ± 0.2 a	1.3 ± 0.2 a	1.6 ± 0.1 a	1.4 ± 0.1 a
Rhamnose	6.1 ± 0.2 a	5.4 ± 0.6 a	6.5 ± 1.1 a	6.2 ± 0.7 a
Arabinose	10.8 ± 2.2 a	11.3 ± 3.1 a	10.8 ± 1.2 a	10.7 ± 1.0 a
Galactose	24.4 ± 6.3 a	23.4 ± 6.8 a	25.0 ± 4.8 a	27.0 ± 2.3 a
Glucose	4.1 ± 0.4 a	2.6 ± 0.6 c	3.6 ± 0.4 ab	3.4 ± 0.4 bc
Xylose	7.0 ± 0.5 a	4.7 ± 1.6 b	7.2 ± 1.2 a	6.0 ± 0.7 ab
Mannose	2.5 ± 0.5 a	1.6 ± 0.6 b	2.1 ± 0.5 ab	1.9 ± 0.1 b
Galacturonic acid	19.2 ± 2.0 b	21.6 ± 5.7 ab	24.4 ± 3.8 a	19.7 ± 1.3 b
Glucuronic acid	0.4 ± 0.2 b	1.2 ± 0 a	0.3 ± 0.1 b	0.1 ± 0 b
Soluble				
Fucose	Bdl	bdl	bdl	bdl
Rhamnose	0.5 ± 0.2 a	0.7 ± 0.1 a	0.6 ± 0.1 a	0.6 ± 0.2 a
Arabinose	1.2 ± 0.3 a	1.5 ± 0.1 a	1.3 ± 0.1 a	1.4 ± 0.2 a
Galactose	2.2 ± 0.7 a	2.7 ± 0.3 a	2.5 ± 0.4 a	2.9 ± 0.7 a
Glucose	2.2 ± 0.8 a	2.5 ± 0.6 a	2.4 ± 0.2 a	2.4 ± 0.4 a
Xylose	0.2 ± 0.1 a	0.3 ± 0 a	0.3 ± 0 a	0.3 ± 0 a
Mannose	0.1 ± 0 a	0.2 ± 0 a	0.1 ± 0 a	0.1 ± 0 a
Galacturonic acid	11.7 ± 2.0 b	13.7 ± 3.6 ab	15.4 ± 3.2 a	15.3 ± 1.6 a
Glucuronic acid	0.1 ± 0	bdl	bdl	bdl

Means ±SD followed by the same letter within each row are not different based on Tukey's Honest Significant Difference test (n=5, P<0.05). Soluble fraction fucose and glucuronic acid were below detectable limit (bdl) of 0.06 μg mg^{-1} AIR.

Table 2. Mean ice nucleation temperatures were observed in non-acclimated, cold acclimated and 50 mM $CaCl_2$ fortified non-acclimated (+ Ca) cells.

	Extrinsic Nucleator	Extracellular Nucleation (°C)	Intracellular Nucleation (°C)
Non-acclimated	–	–8.2 ± 1.1	–8.3 ± 1.1 ^{NS}
	+	–4.1 ± 2.2	–8.4 ± 1.2**
cold acclimated	-	–10.1 ± 2.3	–15.1 ± 4.8**
	+	–3.2 ± 0.9	–21.8 ± 2.4***
Non-acclimated + Ca	-	–9.6 ± 1.8	–9.6 ± 1.7 ^{NS}
	+	–3.1 ± 0.8	–20.7 ± 3.3***

Tissues were cooled in the presence (+) or absence (–) of an extrinsic ice nucleator. Means ±SD within a row were determined to be significantly different using the two-tailed t-test (n=36, NS P>0.05; Asterisks represent significant values; *P<0.05; **P<0.01; ***P<0.001).

temperatures in the Canadian Prairies (Tanino *et al.*, 2013). Our observations of freeze-recovering Japanese bunching onion epidermal cells (Fig. 1) confirm previous findings that exposure to cold acclimation temperatures can significantly lower the LT_{50} to promote overwintering survival (Tanino *et al.*, 2013). Since the epidermal layer is one of the first barriers to ice nucleation and propagation, we predict it plays a significant role in the protection of Japanese bunching onion leaves from freezing injury.

Lethal intracellular freezing in herbaceous leaves can occur if extracellular ice initiates nucleation within the pores of the cell wall (Pearce and Ashworth, 1992; Yamada *et al.*, 2002). Plants can modify cell walls to prevent intracellular ice nucleation (Pearce and Ashworth, 1992; Stegner *et al.*, 2020; Steiner *et al.*, 2020) or whole tissues to mitigate the propagation of ice from sinks into vegetative buds or actively growing organs (Kuprian *et al.*, 2017; Schott *et al.*, 2017). The physical properties of the cell wall and the extracellular (apoplast) space, therefore, is essential to the avoidance of intracellular ice nucleation (George and Burke, 1977; Ashworth and Abeles, 1984; Wisniewski and Davis, 1995; Yamada *et al.*, 2002). The reduced porosity and decreased permeability of the cell wall would play an essential role in blocking ice propagation from the extracellular to the intracellular space. In Japanese bunching onion we assessed the effect of cold acclimation on pore size using a fluorescein molecule with an effective radius of 6.5 Å (equal to 1.3 nm in diameter; Lawrence *et al.*, 1994) and as small as 5.02 Å (Mustafa *et al.*, 1993). It is possible that exposure to 12/4 °C prior to experimentation induces a lower endocytosis activity and fluorescence dye internalization (Bolte *et al.*, 2004). Epidermal peels were collected from cold acclimated Japanese bunching onion held at 20 °C for a minimum of 0.5 h prior to analysis.

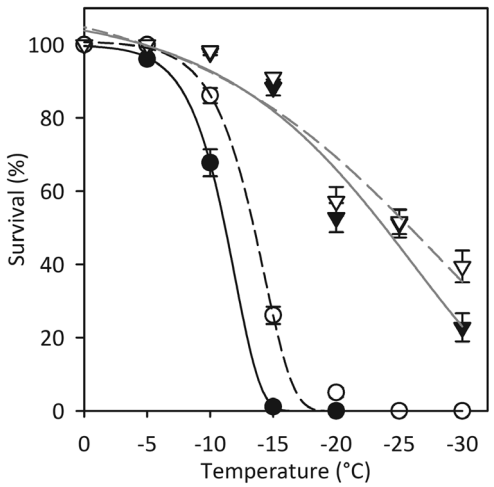

Fig. 5. Effect of exogenous calcium on the freezing survival of epidermal cells. The survival rate of epidermal cells collected from non-acclimated (closed circle), non-acclimated exposed to a weekly 50 mM $CaCl_2$ nutrient treatment (+ Ca) (open circle), cold acclimated (closed inverted triangle) or cold acclimated + Ca (open inverted triangle) Japanese bunching onions. The Gompertz function was used to calculate the lethal temperature at which half the cells survived freezing in non-acclimated (–10.5 °C), non-acclimated + Ca (–12.9 °C), cold acclimated (–23.7 °C) and cold acclimated + Ca (–26.0 °C) epidermal cells. Data are means ±SD (n=5).

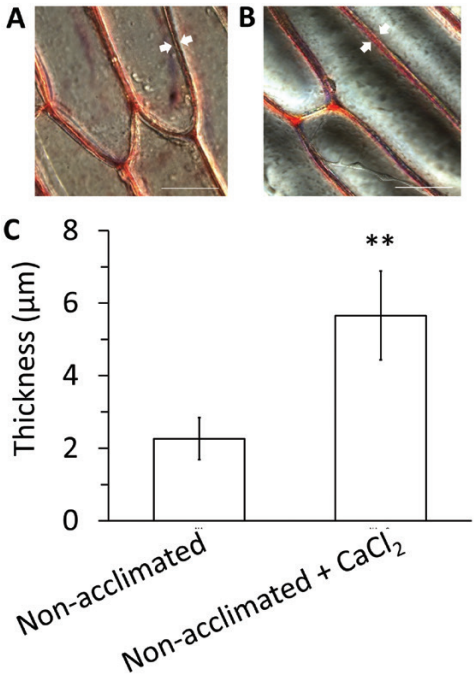

Fig 6. The deposition of crimson precipitates associated with Ca^{2+} deposition in the cell wall following $CaCl_2$ treatment. Single-cell layer collected from (A) non-acclimated control or (B) with 50 mM $CaCl_2$ treated plants stained with Alizarin red S. Thickness of the Ca^{2+} deposition region is marked by the white arrows. Scale bar =50 µm. (C) Mean thickness ±SE were assessed for statistical significance (n=4, two-tailed t-test. Asterisks represent significant values, **, P<0.01).

The cold acclimation-induced decline in cell wall permeability suggests that pore diameters in cold acclimated Japanese bunching onion were reduced to at least 1.3 nm (Fig. 2) and corroborates previous studies observing reduced permeability in the buds of dormant Norway spruce (Lee *et al.*, 2017) and cold acclimated peach (Wisniewski *et al.*, 1987). Future cold acclimation and calcium dose response measurements using dextran-fluorescein labelling along with chelation experiments, would provide additional validation and insights.

Cold acclimation promotes cell wall remodelling

Exposure of Japanese bunching onion to 12/4 °C for 14 d enhanced total cell wall dry mass (Fig. 3A) and was associated with a greater accumulation of soluble and insoluble galacturonic acid (Table 1), which is in agreement with observations in the leaves of winter rape (Kubacka-Zębalska and Kacperska, 1999; Solecka *et al.*, 2008), Arabidopsis (Takahashi *et al.*, 2019) and pea (Baldwin *et al.*, 2014). Interestingly, we did not see a greater accumulation of arabinose or galactose (Table 1), which in pea leaves arises from an accumulation of arabinan or arabinogalactan side chains associated with the modification of RG-I and enhanced frost tolerance (Baldwin *et al.*, 2014). We also did not observe a shift in cell wall fucose concentrations (Table 1) which was previously observed in Arabidopsis to be linked with the dimerization of RG-II with B^+ and diminished freezing tolerance (Panter *et al.*, 2019). The reduction of glucose in the cell walls of cold acclimated and $CaCl_2$ supplemented Japanese bunching onion, and a reduction in 1350 to 1315 cm^{-1} and 970 cm^{-1} associated with cellulose (Table 1), supports previous observations in the leaves of winter rape (Kubacka-Zębalska and Kacperska, 1999) that a relative reduction in cellulose is associated with the remodelling of cold acclimated herbaceous cell walls.

The activity of Japanese bunching onion epidermal PME was significantly higher in response to cold acclimation (Fig. 3B-D), which is reflected by a lower amount of methyl esterified pectins, as confirmed by JIM5 immunolabelling (Fig. 4A) and a reduction in 1740 cm^{-1} peak intensity (Fig. 4D). These results support our previous observations that characterize a reduction in methyl esterification after exposure to 10/5 °C for 14 d (Tanino *et al.*, 2013). Similarly, Solecka *et al.* (2008) reported greater JIM5 immunolabelling in cross-sections from cold acclimated winter rape leaves. Taken together with our XAS spectra (Supplementary Fig. S3), the theory that a decline in the degree of Japanese bunching onion epidermal cell methylation corresponds with the crosslinking of HG with Ca^{2+} is supported.

Pectin-mediated regulation of porosity and permeability is an attractive hypothesis because it explains the formation of pectin-fortified tissue-level barriers to ice propagation between frozen and supercooled tissues (Wisniewski and Davis, 1995; Kuprian *et al.*, 2017), and may play a role in the vascular de-segmentation observed in overwintering buds to promote

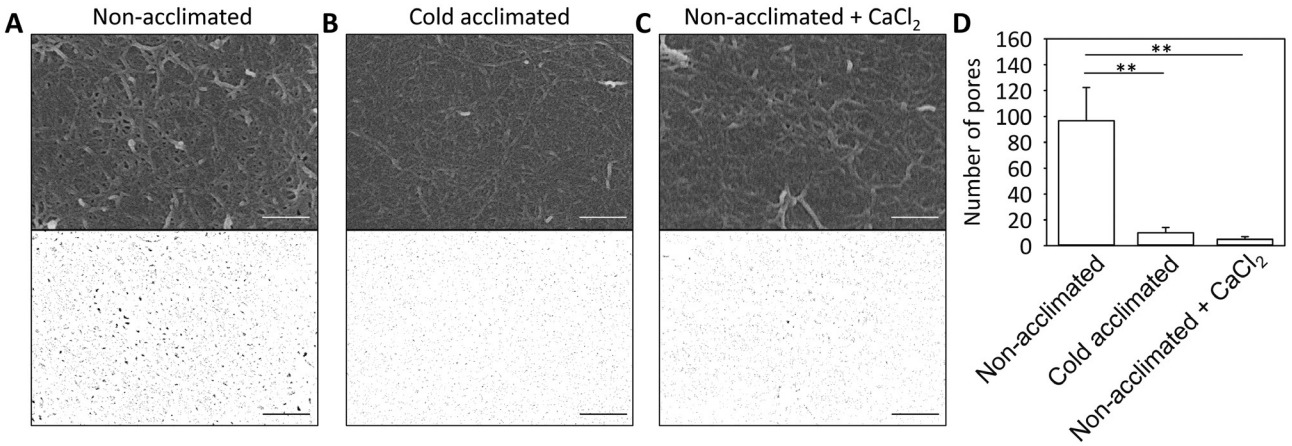

Fig. 7. Scanning electron micrographs of the surface of a single epidermal cell layer. Epidermal peels were collected from (A) non-acclimated, (B) cold acclimated and (C) non-acclimated plants treated with 50 mM $CaCl_2$. Representative images depict the micrograph (top) and a false-colour image generated using ImageJ (lower) to visualize pores with a minimum threshold of 15 pixels. (D) The mean number of pores ±SE were assessed for statistical significance (n=4, two-tailed t-test; asterisks represent significant values, **, P<0.01). The grey images are the original images obtained, and the white images were processed using the threshold function in ImageJ to visualize pores larger than 15 pixels. Scale bar =200 nm.

dormancy (Lee *et al.*, 2017). George and Burke (1977) proposed an 'ink bottle effect' to explain why the comparatively smaller diameters of cell wall microcapillaries facilitate the establishment of a vapour pressure equilibrium between supercooled intracellular water and the extracellular or extrinsic ice aggregate.

In cold acclimated Japanese bunching onion, the reductions in pore number, as observed with SEM imaging (Fig. 7) and reduced tissue permeability to fluorescein (Fig. 2), supports the theory that cold acclimation reduces pore size. Furthermore, by manipulating the cross-linking of Ca^{2+} with HG, our data are in agreement with observations from cold acclimated xylem ray parenchyma cells of peach (Wisniewski *et al.*, 1991; Wisniewski and Davis, 1995). It was also previously observed that exogenous application of Ca^{2+} chelators, and to a lesser extent pectinase, degraded the outer two layers of the pore pit membrane, partially degraded an amorphous layer of pectin within the xylem parenchyma cell, and shifted the low-temperature exotherm associated with intracellular freezing to a warmer temperature (Wisniewski *et al.*, 1991). The modification of HG methyl esterification status can influence resistance to tensile and compressive stresses induced during cell expansion (Cosgrove, 2018; Wang *et al.*, 2020), pathogenic (Lionetti *et al.*, 2012) or osmotic stress, or dehydration injury (Chen *et al.*, 2018). We hypothesize that modifications to pectin cell wall methyl esterification status are a general acclimation mechanism, that in certain plant tissues can protect cells against freezing injury and other environmental stressors through an increased barrier.

Reduction in pore size reduces intracellular ice nucleation temperature

The application of $CaCl_2$ to non-acclimated plants reduces intracellular ice nucleation temperatures by 12 °C (<–20 °C; Table 2). Light microscopy images characterizing greater deposition Ca^{2+} in the primary cell wall (Fig. 6) corresponded with visual observations of cell wall ultrastructure (Figs 7, 8). In cold acclimated bunching onion epidermal cells, we observed that exogenous application of $CaCl_2$ modified the depositional properties of the cell wall (via transmission electron microscopy; Fig. 8), reduced the number of large cell wall pores (via scanning electron microscopy; Fig. 7) while reducing the lethal intracellular ice nucleation temperature (Table 2).

Extrinsic nucleation with silver iodide elevated the extracellular ice nucleation temperature in Japanese bunching onion treated with 50 mM $CaCl_2$ or grown under cold acclimated conditions (Table 2). Lower intracellular ice nucleation temperatures are likely a function of the reduced energy of ice propagation (Olien, 1974; Olien and Livingston, 2006) and a small pore size induced by the cross-linking of HG with Ca^{2+}. This combined response inhibits the propagation of ice from the extracellular space into the intracellular space and is necessary for the development of a vapour pressure gradient (see review by Takahashi *et al.*, 2021*b*). Supercooling of extracellular water to a lower temperature followed by sudden freezing results in a higher energy of ice propagation, enabling ice to physically cross the cell wall and plasma membrane barrier (Asahina, 1956; Ashworth and Abeles, 1984; Olien and Livingston, 2006). This may explain why extrinsically nucleated epidermal cells collected from plants grown under non-acclimated conditions with a 50 mM $CaCl_2$ treatment develop low intracellular ice nucleation temperatures.

We observed using Alizarin red staining that non-acclimated Japanese bunching onions supplemented with 50 mM $CaCl_2$ visibly accumulated more crimson precipitates associated with Ca^{2+} deposition within the cell wall region (Fig. 6), suggesting that Ca^{2+} supplementation may augment cell wall composition. Our observations agree with observations in $CaCl_2$ fortified spinach (*Spinacia oleracea* L. 'Reflect') that accumulates

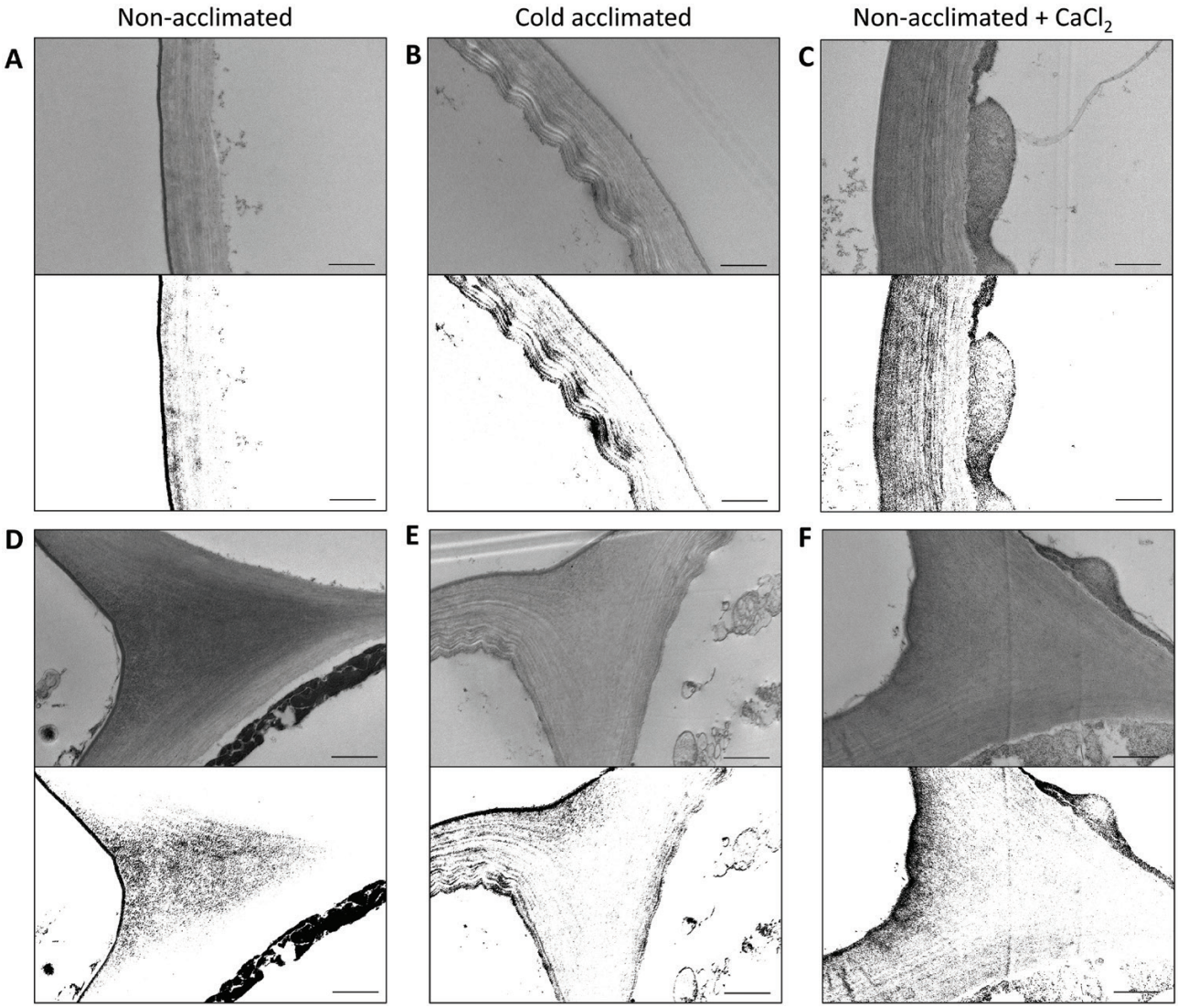

Fig. 8. Transmission electron micrographs of cell wall in a single epidermal cell layer. Micrographs were collected from (A, D) non-acclimated, (B, E) cold acclimated and (C, F) non-acclimated plants treated with 50 mM $CaCl_2$. Each upper panel illustrates a transmission micrograph (A, B, C) of the side wall. (D, E, F) Lower panels illustrate the tricellular junction. Representative samples based on four replications are shown. The grey images are the original images obtained, and the white images were processed using the threshold function in ImageJ to visualize lines in cell layer. Scale bars =1 μm.

higher amounts of cell wall dry matter and cell wall Ca^{2+} (Min *et al.*, 2021). Supplementation of Ca^{2+} in potatoes (*Solanum tuberosum* L.) enhanced the total fraction of soluble pectin and cell wall Ca^{2+} in tubers (Murayama *et al.*, 2017). While there is no known threshold for the amount of Ca^{2+} required for onion cell walls to develop Ca^{2+} cross linkages, sub-optimal concentrations of Ca^{2+} can reduce gel stiffness and promote the disassociation of Ca^{2+} crosslinks (Tibbits *et al.*, 1998). Common onion cells de-methylesterified by PME in the absence of exogenous Ca^{2+} promotes swelling and not the rigidification of the cell wall (Wang *et al.*, 2020). Ripening of the fruit pericarp is linked to the de-methylesterification of HG, and physiological disorders such as blossom end rot associated with a lack of extracellular Ca^{2+} can be mitigated through the foliar application of Ca^{2+} (de Freitas *et al.*, 2012). *In vitro* studies identified that PME isolated from orange peels have a higher activity in the presence of 5 mM $CaCl_2$, as opposed to experiments lacking calcium (Videcoq *et al.*, 2011). In the present study, the accumulation of Ca^{2+} induced by $CaCl_2$ application likely mimics the cold acclimation-triggered exudation of Ca^{2+} to the extracellular space and plasma membrane. Higher concentrations of extracellular Ca^{2+} from exogenous or cold-induced intracellular trafficking likely promote greater cross-linking of HG with Ca^{2+} in the Japanese bunching onion cell wall.

Although the application of $CaCl_2$ to non-acclimated plants reduces intracellular ice nucleation temperatures by 12 °C (<–20°C), the LT_{50} was only reduced by 2 °C (–14 °C;

Table 2). Prolonged exposure of supercooled plant cells to sub-zero temperatures can induce chilling injury. The cold acclimated and $CaCl_2$-treated Japanese bunching onion freezing tolerant cells must also have a degree of intracellular chilling tolerance to avoid lethal membrane injury, as was previously observed in orchid (*Paphiopedilum insigne* [Wallich ex Lindl.] Pfitz.) leaves (Yamada *et al.*, 2002); thus the limiting factor may be the lack of chilling tolerance in $CaCl_2$-treated plants.

Our $CaCl_2$ fortification results do not preclude the possibility that the 2–3 °C shift in LT_{50} is a result of calcium signalling. Calcium plays a key role as a secondary messenger for a wide range of stresses, including light, touch, pathogens, salinity, cold, and drought (Tuteja and Mahajan, 2007). Exogenous application of $CaCl_2$ to potatoes ameliorates yield penalties induced by soil NaCl (Etehadnia *et al.*, 2010). Hiraki *et al.* (2019) demonstrated greater induction of endogenous calcium signalling linked to dehydration-responsive element-binding protein (DREBs)/C-repeat-binding factors (CBFs) when Arabidopsis was exposed to natural diurnal field-based temperature shifts. Our $CaCl_2$ fortification results do not preclude the possibility that the 2–3 °C shift in LT_{50} is also a result of higher Ca^{2+} associated with the plasma membrane. Freezing-induced plasma membrane injury and leakage of K^+ in cold acclimated common onion epidermal cells (Palta *et al.*, 1977) is associated with diminished plasma membrane H^+-ATPase activity (Arora and Palta, 1991). Impairment of transport and permeability of the plasma membrane facilitates the passive influx of K^+ and water into the cell, enhancing protoplasmic swelling (Arora and Palta, 1986). Supplementation with $CaCl_2$ mitigates membrane Ca^{2+} loss by extracellular K^+ and reduces membrane and tissue injury in onion (Arora and Palta, 1986, 1988) and spinach (Min *et al.*, 2021). While we did not assess ion leakage in Japanese bunching onion epidermal cells, our fluorescence stains quantified membrane permeability after a freeze-thaw injury. Treatment of non-acclimated plants with $CaCl_2$ may ameliorate K^+ induced plasma membrane injury. The use of a 5 °C h^{-1} cooling rate could promote injury at warmer temperatures, as cooling rates of less than 3 °C h^{-1} were observed to reduce freezing injury in common onion epidermal cells (Steffen *et al.*, 1989). This may explain why there was only a 2 °C difference in LT_{50} between non-acclimated Japanese bunching onions with or without $CaCl_2$ supplementation. The $CaCl_2$ fortification of non-acclimated cells supports the theory that the plasma membrane, through dehydration or freeze-thaw injury, limits the tolerance of Japanese bunching onion to freezing injury (Arora, 2018). Additional research is needed to compare whether a 2.5 °C h^{-1} or 5 °C h^{-1} cooling rate influences the degree of injury in epidermal cells harvested from the comparatively more freezing tolerant Japanese bunching onion, and the comparatively less tolerant common onion.

In conclusion, our studies have explored the consequences of $CaCl_2$ and cold acclimation on isolated Japanese bunching onion cell wall composition, ultrastructure, and its influence on ice nucleation. Greater PME activity in cold acclimated plants de-methyl esterified HG, as observed with JIM5 immunolabeling and FTIR. Our XAS spectra and transmission electron microscopy support the theory that acidified HG is covalently cross-linked with Ca^{2+}. This corresponds with the accumulation of cell wall dry matter driven by higher concentrations of galacturonic acid and reduced tissue permeability, as measured with fluorescein. In a separate experiment, the exogenous application of $CaCl_2$ to non-acclimated Japanese bunching onion mimics the cold acclimated induced cell wall remodelling in epidermal cells. Japanese bunching onion either supplemented with 50 mM $CaCl_2$ while grown under non-acclimated or cold acclimated conditions, developed smaller pores and undulating tissue layers, as observed with electron microscopy. Similarly, the non-acclimated $CaCl_2$ supplemented, and cold acclimated plants maintain high extracellular ice nucleation temperatures (–4 °C) and intracellular ice nucleation temperatures lower than –20 °C, suggesting that reductions in pore size via HG Ca^{2+} crosslinking lowers lethal intracellular ice nucleation temperatures. Avoidance of intracellular freezing and enhanced supercooling may be particularly beneficial to frost-sensitive plants and organs. Nominal differences in the LT_{50} of non-acclimated plants with or without $CaCl_2$ supplementation suggests that the survival of freezing tolerant Japanese bunching onion leaves is limited not by the cell wall but the capacity of the plasma membrane to tolerate freezing dehydration, chilling and thawing injury.

Supplementary data

The following supplementary data are available at *JXB* online.

Fig. S1. Cell wall protein content isolated from the onion epidermal, non-epidermal and whole sheath after exposure to 12/4 °C for 0, 3, 7 and 14 d.

Fig. S2. Application of principal components (PC) analysis to the fingerprint region (1800–900 cm^{-1}) of Fourier-transformed infrared (FTIR) spectra collected from the epidermal cell wall region of non (NA) and cold acclimated (ACC) Japanese onions.

Fig. S3. XAS Ca^{2+} spectra isolated from non (NA) and cold acclimated (ACC) cell walls.

Video S1. Visualization of freezing in non-acclimated cells without extracellular nucleation.

Video S2. Visualization of freezing in non-acclimated cells treated for 4 weeks with 50 mM $CaCl_2$ without extracellular ice nucleation.

Acknowledgements

We thank Eiko Kawamura and Larhonda Sobchishin (University of Saskatchewan, Canada) for assistance with electron microscopy and Ricky Lee (University of Saskatchewan, Canada) for guidance on the cryostage; Rachid Lahlali, Vijayan Perumal, Ferenc Borondics, Xia Liu and Saroj Kumar (Canadian Light Source, Canada) for help in collecting

FTIR spectra; Matsuo Uemura, Yukio Kawamura, Abidur Rahman (Iwate University, Japan), Yuguang Bai, Gord Gray and Monica Baga (University of Saskatchewan, Canada), Michael Wisniewski (USDA-ARS) and Trine Hvoslef-Eide (Norwegian University of Life Sciences, Norway) for inciteful discussions; Eldon Siemens, Lei Ren as well as fellow lab members Jihua Xu, Pankaj Banik and Eric Rae for their support and assistance (University of Saskatchewan, Canada).

Author contributions

KKT designed the experiments; JL, HH, ADF, JRL, GDWS, YW, SG, BU, AW, MG, YL, JEO, CK and JD performed the experiments; JL, IRW, HH, CK, and ADF analysed the data; IRW and JL wrote the manuscript. IRW and KKT edited the manuscript with contributions from all authors.

Conflict of interest

The authors declare that there is no conflict of interest.

Funding

This work was supported by a China Scholarship Council grant to JL and a Natural Sciences and Engineering Research Council of Canada grant to KKT. Part of the research was performed at the Canadian Light Source, which is funded by the Canada Foundation for Innovation, the Natural Sciences and Engineering Research Council, the National Research Council, the Canadian Institutes of Health Research, the Government of Saskatchewan, and the University of Saskatchewan.

Data availability

Data supporting the findings of this study are available within the paper and supplementary data published online.

References

Alonso-Simón A, García-Angulo P, Mélida H, Encina A, Álvarez JM, Acebes JL. 2011. The use of FTIR spectroscopy to monitor modifications in plant cell wall architecture caused by cellulose biosynthesis inhibitors. Plant Signaling & Behavior **6**, 1104–1110.

Arora R. 2018. Mechanism of freeze-thaw injury and recovery: a cool retrospective and warming up to new ideas. Plant Science **270**, 301–313.

Arora R, Palta JP. 1986. Protoplasmic swelling as a symptom of freezing injury in onion bulb cells: its simulation in extracellular KCl and prevention by calcium. Plant Physiology **82**, 625–629.

Arora R, Palta JP. 1988. *In vivo* perturbation of membrane-associated calcium by freeze-thaw stress in onion bulb cells: simulation of this perturbation in extracellular KCl and alleviation by calcium. Plant Physiology **87**, 622–628.

Arora R, Palta JP. 1991. A loss in the plasma membrane ATPase activity and its recovery coincides with incipient freeze-thaw injury and post-thaw recovery in onion bulb scale tissue. Plant Physiology **95**, 846–852.

Asahina E. 1956. The freezing process of plant cell. Contributions from the Institute of Low Temperature Science **10**, 83–126.

Ashworth EN, Abeles FB. 1984. Freezing behavior of water in small pores and the possible role in the freezing of plant tissues. Plant Physiology **76**, 201–204.

Atmodjo MA, Hao Z, Mohnen D. 2013. Evolving views of pectin biosynthesis. Annual Review of Plant Biology **64**, 747–779.

Baldwin L, Domon JM, Klimek JF, Fournet F, Sellier H, Gillet F, Pelloux J, Lejeune-Hénaut I, Carpita NC, Rayon C. 2014. Structural alteration of cell wall pectins accompanies pea development in response to cold. Phytochemistry **104**, 37–47.

Bolte S, Talbot C, Boutte Y, Catrice O, Read ND, Satiat-Jeunemaitre B. 2004. FM-dyes as experimental probes for dissecting vesicle trafficking in living plant cells. Journal of Microscopy **214**, 159–173.

Chatjigakis AK, Pappas C, Proxenia N, Kalantzi O, Rodis P, Polissiou M. 1998. FT-IR spectroscopic determination of the degree of esterification of cell wall pectins from stored peaches and correlation to textural changes. Carbohydrate Polymers **37**, 395–408.

Chen J, Chen X, Zhang Q, Zhang Y, Ou X, An L, Feng H, Zhao Z. 2018. A cold-induced pectin methyl-esterase inhibitor gene contributes negatively to freezing tolerance but positively to salt tolerance in Arabidopsis. Journal of Plant Physiology **222**, 67–78.

Clausen MH, Willats WG, Knox JP. 2003. Synthetic methyl hexagalacturonate hapten inhibitors of anti-homogalacturonan monoclonal antibodies LM7, JIM5 and JIM7. Carbohydrate Research **338**, 1797–1800.

Cosgrove DJ. 2018. Diffuse growth of plant cell walls. Plant Physiology **176**, 16–27.

Cosmidis J, Benzerara K, Nassif N, Tyliszczak T, Bourdelle F. 2015. Characterization of Ca-phosphate biological materials by scanning transmission X-ray microscopy (STXM) at the Ca L2,3-, P L2,3- and C K-edges. Acta Biomaterialia **12**, 260–269.

de Freitas ST, Handa AK, Wu Q, Park S, Mitcham EJ. 2012. Role of pectin methylesterases in cellular calcium distribution and blossom-end rot development in tomato fruit. The Plant Journal **71**, 824–835.

Etehadnia M, Schoenau J, Waterer D, Tanino KK. 2010. The effect of $CaCl_2$ and NaCl salt acclimation in stress tolerance and its potential role in ABA and scion/rootstock-mediated salt stress responses. Plant Stress **4**, 72–81.

Foster CE, Martin TM, Pauly M. 2010. Comprehensive compositional analysis of plant cell walls (lignocellulosic biomass) part II: carbohydrates. Journal of Visualized Experiments: JoVE **37**, 1837.

George MF, Burke MJ. 1977. Cold hardiness and deep supercooling in xylem of shagbark hickory. Plant Physiology **59**, 319–325.

Griffith M, Huner NP, Espelie KE, Kolattukudy PE. 1985. Lipid polymers accumulate in the epidermis and mestome sheath cell walls during low temperature development of winter rye leaves. Protoplasma **125**, 53–64.

Gusta LV, Wisniewski M. 2013. Understanding plant cold hardiness: an opinion. Physiologia Plantarum **147**, 4–14.

Hiraki H, Uemura M, Kawamura Y. 2019. Calcium signaling-linked CBF/DREB1 gene expression was induced depending on the temperature fluctuation in the field: views from the natural condition of cold acclimation. Plant & Cell Physiology **60**, 303–317.

Jones KS, McKersie BD, Paroschy JH. 2000. Prevention of ice propagation by permeability barriers in bud axes of *Vitis vinifera*. Canadian Journal of Botany **78**, 3–9.

Kovaleski AP, Grossman JJ. 2021. Standardization of electrolyte leakage data and a novel liquid nitrogen control improve measurements of cold hardiness in woody tissue. Plant Methods **17**, 53.

Kubacka-Zębalska M, Kacperska A. 1999. Low temperature-induced modifications of cell wall content and polysaccharide composition in leaves of winter oilseed rape (*Brassica napus* L. var. *oleifera* L.). Plant Science **148**, 59–67.

Kuprian E, Munkler C, Resnyak A, Zimmermann S, Tuong TD, Gierlinger N, Müller T, Livingston DP 3rd, Neuner G. 2017. Complex bud architecture and cell-specific chemical patterns enable supercooling of *Picea abies* bud primordia. Plant, Cell & Environment **40**, 3101–3112.

Lawrence JR, Wolfaardt GM, Korber DR. 1994. Determination of diffusion coefficients in biofilms by confocal laser microscopy. Applied and Environmental Microbiology **60**, 1166–1173.

Lee Y, Derbyshire P, Knox JP, Hvoslef-Eide AK. 2008. Sequential cell wall transformations in response to the induction of a pedicel abscission event in *Euphorbia pulcherrima* (poinsettia). The Plant Journal **54**, 993–1003.

Lee Y, Karunakaran C, Lahlali R, Liu X, Tanino KK, Olsen JE. 2017. Photoperiodic regulation of growth-dormancy cycling through induction of multiple bud-shoot barriers preventing water transport into the winter buds of Norway spruce. Frontiers in Plant Science **8**, 2109.

Lionetti V, Cervone F, Bellincampi D. 2012. Methyl esterification of pectin plays a role during plant-pathogen interactions and affects plant resistance to diseases. Journal of Plant Physiology **169**, 1623–1630.

Liu J. 2015. Temperature-mediated alterations of the plant apoplast as a mechanism of intracellular freezing stress avoidance. University of Saskatchewan. MSc Thesis.

Meents MJ, Watanabe Y, Samuels AL. 2018. The cell biology of secondary cell wall biosynthesis. Annals of Botany **121**, 1107–1125.

Min K, Liu B, Lee S-R, Arora R. 2021. Supplemental calcium improves freezing tolerance of spinach (*Spinacia oleracea* L.) by mitigating membrane and photosynthetic damage, and bolstering anti-oxidant and cell-wall status. Scientia Horticulturae **288**, 110212.

Mohnen D, Engle KA, Amos RA, Yan J-Y, Glushka J, Atmodjo M, Tan L, Moremen KW. 2021. A new model for pectin structure and synthesis. Plant Cell Wall Biology 2021, Abstract p. 59. Japan.

Murai M, Yoshida S. 1998. Evidence for the cell wall involvement in temporal changes in freezing tolerance of Jerusalem artichoke (*Helianthus tuberosus* L.) tubers during cold acclimation. Plant & Cell Physiology **39**, 97–105.

Murayama D, Tani M, Ikeda S, Palta JP, Pelpolage SW, Yamauchi H, Koaze H. 2017. Effects of calcium concentration in potato tuber cells on the formation of cross-links between pectin molecules by Ca^{2+}. American Journal of Potato Research **94**, 524–533.

Mustafa MB, Tipton DL, Barkley MD, Russo PS, Blum FD. 1993. Dye diffusion in isotropic and liquid-crystalline aqueous (hydroxypropyl) cellulose. Macromolecules **26**, 370–378.

Olien CR. 1974. Energies of freezing and frost desiccation. Plant Physiology **53**, 764–767.

Olien CR, Livingston DP. 2006. Understanding freeze stress in biological tissues: Thermodynamics of interfacial water. Thermochimica Acta **451**, 52–56.

Palta JP, Levitt J, Stadelmann EJ. 1977. Freezing injury in onion bulb cells: I. Evaluation of the conductivity method and analysis of ion and sugar efflux from injured cells. Plant Physiology **60**, 393–397.

Panter PE, Kent O, Dale M, *et al.* 2019. MUR1-mediated cell-wall fucosylation is required for freezing tolerance in Arabidopsis thaliana. New Phytologist **224**, 1518–1531.

Park YB, Cosgrove DJ. 2015. Xyloglucan and its interactions with other components of the growing cell wall. Plant & Cell Physiology **56**, 180–194.

Paul H, Reginato AJ, Schumacher HR. 1983. Alizarin red S staining as a screening test to detect calcium compounds in synovial fluid. Arthritis and Rheumatism **26**, 191–200.

Pearce RS, Ashworth EN. 1992. Cell shape and localisation of ice in leaves of overwintering wheat during frost stress in the field. Planta **188**, 324–331.

Phyo P, Wang T, Kiemle SN, O'Neill H, Pingali SV, Hong M, Cosgrove DJ. 2017. Gradients in wall mechanics and polysaccharides along growing inflorescence stems. Plant Physiology **175**, 1593–1607.

Rajashekar CB, Lafta A. 1996. Cell-wall changes and cell tension in response to cold acclimation and exogenous abscisic acid in leaves and cell cultures. Plant Physiology **111**, 605–612.

Regier T, Krochak J, Sham TK, Hu YF, Thompson J, Blyth RI. 2007. Performance and capabilities of the Canadian Dragon: The SGM beamline at the Canadian Light Source. Nuclear Instruments and Methods in Physics Research Section A: Accelerators, Spectrometers, Detectors and Associated Equipment **582**, 93–95.

Richard L, Qin LX, Gadal P, Goldberg R. 1994. Molecular cloning and characterisation of a putative pectin methylesterase cDNA in *Arabidopsis thaliana* (L.). FEBS Letters **355**, 135–139.

Sakai A, Larcher W. 1987. *Frost survival of plants: responses and adaptation to freezing stress*. In Ecological Studies Vol **62**. Springer-Verlag: Berlin Heidelberg. 321 pp.

Schott RT, Voigt D, Roth-Nebelsick A. 2017. Extracellular ice management in the frost hardy horsetail *Equisetum hyemale* L. Flora **234**, 207–214.

Shi Y, Ding Y, Yang S. 2018. Molecular regulation of CBF signaling in cold acclimation. Trends in Plant Science **23**, 623–637.

Siminovitch D, Singh J, De la Roche IA. 1978. Freezing behavior of free protoplasts of winter rye. Cryobiology **15**, 205–213.

Solecka D, Zebrowski J, Kacperska A. 2008. Are pectins involved in cold acclimation and de-acclimation of winter oil-seed rape plants? Annals of Botany **101**, 521–530.

Steffen KL, Arora R, Palta JP. 1989. Relative sensitivity of photosynthesis and respiration to freeze-thaw stress in herbaceous species: importance of realistic freeze-thaw protocols. Plant Physiology **89**, 1372–1379.

Stegner M, Lackner B, Schäfernolte T, Buchner O, Xiao N, Gierlinger N, Holzinger A, Neuner G. 2020. Winter nights during summer time: stress physiological response to ice and the facilitation of freezing cytorrhysis by elastic cell wall components in the leaves of a nival species. International Journal of Molecular Sciences **21**, 7042.

Steiner P, Obwegeser S, Wanner G, Buchner O, Lütz-Meindl U, Holzinger A. 2020. Cell wall reinforcements accompany chilling and freezing stress in the streptophyte green alga *Klebsormidium crenulatum*. Frontiers in Plant Science **11**, 873.

Szymanska-Chargot M, Zdunek A. 2013. Use of FT-IR spectra and PCA to the bulk characterization of cell wall residues of fruits and vegetables along a fraction process. Food Biophysics **8**, 29–42.

Takahashi D, Gorka M, Erban A, Graf A, Kopka J, Zuther E, Hincha DK. 2019. Both cold and sub-zero acclimation induce cell wall modification and changes in the extracellular proteome in *Arabidopsis thaliana*. Scientific Reports **9**, 2289.

Takahashi D, Johnson KL, Hao P, *et al.* 2021a. Cell wall modification by the xyloglucan endotransglucosylase/hydrolase XTH19 influences freezing tolerance after cold and sub-zero acclimation. Plant, Cell & Environment **44**, 915–930.

Takahashi D, Uemura M, Kawamura Y. 2018. Freezing tolerance of plant cells: from the aspect of plasma membrane and microdomain. Advances in Experimental Medicine and Biology **1081**, 61–79.

Takahashi D, Willick IR, Kasuga J, Livingston Iii DP. 2021b. Responses of the plant cell wall to sub-zero temperatures: a brief update. Plant & Cell Physiology **62**, 1858–1866.

Tanino KK, Chen THH, Fuchigami LH, Weiser CJ. 1990. Metabolic alterations associated with abscisic acid-induced frost hardiness in bromegrass suspension culture cells. Plant & Cell Physiology **31**, 505–511.

Tanino KK, Kobayashi S, Hyett C, *et al.* 2013. *Allium fistulosum* as a novel system to investigate mechanisms of freezing resistance. Physiologia Plantarum **147**, 101–111.

Tibbits CW, MacDougall AJ, Ring SG. 1998. Calcium binding and swelling behaviour of a high methoxyl pectin gel. Carbohydrate Research **310**, 101–107.

Tuteja N, Mahajan S. 2007. Calcium signaling network in plants: an overview. Plant Signaling & Behavior **2**, 79–85.

Videcoq P, Garnier C, Robert P, Bonnin E. 2011. Influence of calcium on pectin methylesterase behaviour in the presence of medium methylated pectins. Carbohydrate Polymers **86**, 1657–1664.

Wang T, Park YB, Cosgrove DJ, Hong M. 2015. Cellulose-pectin spatial contacts are inherent to never-dried Arabidopsis primary cell walls: evidence from solid-state nuclear magnetic resonance. Plant Physiology **168**, 871–884.

Wang X, Wilson L, Cosgrove DJ. 2020. Pectin methylesterase selectively softens the onion epidermal wall yet reduces acid-induced creep. Journal of Experimental Botany **71**, 2629–2640.

Weiser C. 1970. Cold resistance and injury in woody plants: knowledge of hardy plant adaptations to freezing stress may help us to reduce winter damage. Science **169**, 1269–1278.

White PB, Wang T, Park YB, Cosgrove DJ, Hong M. 2014. Water-polysaccharide interactions in the primary cell wall of *Arabidopsis thaliana* from polarization transfer solid-state NMR. Journal of the American Chemical Society **136**, 10399–10409.

Willats WG, Orfila C, Limberg G, *et al.* 2001. Modulation of the degree and pattern of methyl-esterification of pectic homogalacturonan in plant cell walls: implications for pectin methyl esterase action, matrix properties, and cell adhesion. Journal of Biological Chemistry **276**, 19404–19413.

Willick IR, Stobbs J, Karunakaran C, Tanino KK. 2020. Phenotyping plant cellular and tissue level responses to cold with synchrotron-based fourier-transform infrared spectroscopy and X-ray computed tomography. Methods in Molecular Biology **2156**, 141–159.

Willick IR, Takahashi D, Fowler DB, Uemura M, Tanino KK. 2018. Tissue-specific changes in apoplastic proteins and cell wall structure during cold acclimation of winter wheat crowns. Journal of Experimental Botany **69**, 1221–1234.

Wisniewski M, Ashworth E, Schaffer K. 1987. The use of lanthanum to characterize cell wall permeability in relation to deep supercooling and extracellular freezing in woody plants. Protoplasma **139**, 105–116.

Wisniewski M, Davis G. 1995. Immunogold localization of pectins and glycoproteins in tissues of peach with reference to deep supercooling. Trees **9**, 253–260.

Wisniewski M, Davis G, Arora R. 1991. Effect of macerase, oxalic acid, and EGTA on deep supercooling and pit membrane structure of xylem parenchyma of peach. Plant Physiology **96**, 1354–1359.

Xiao C, Zhang T, Zheng Y, Cosgrove DJ, Anderson CT. 2016. Xyloglucan deficiency disrupts microtubule stability and cellulose biosynthesis in Arabidopsis, altering cell growth and morphogenesis. Plant Physiology **170**, 234–249.

Yamada T, Kuroda K, Jitsuyama Y, Takezawa D, Arakawa K, Fujikawa S. 2002. Roles of the plasma membrane and the cell wall in the responses of plant cells to freezing. Planta **215**, 770–778.

Zamil MS, Geitmann A. 2017. The middle lamella-more than a glue. Physical Biology **14**, 015004.